한국기계가공학회지, 제20권, 제1호, pp. 7～15(2021.01) ISSN 1598-6721(Print)
Journal of the Korean Society of Manufacturing Process Engineers, Vol. 20, No. 1, pp. 7~15(2021.01) ISSN 2288-0771(Online)

https://doi.org/10.14775/ksmpe.2021.20.01.007

Thermal Impact Evaluation on Buckling of Cylindrical Structures Using Shell Elements

Hee-Keun Cho*,#

*School of Mechanical Engineering Education, Andong National Univ.

쉘요소를 활용한 원통형 구조물의 좌굴에 대한 열적 영향평가

조희근*,#

*국립안동대학교 기계교육과

(Received 28 September 2020; received in revised form 10 November 2020; accepted 14 November 2020)

ABSTRACT

Buckling of cylindrical structures has been extensively researched, because it is an important phenomenon to be considered in structural design. However, the evaluation of thermal effects on the buckling of cylindrical structures has been insufficient; therefore, this study evaluates this thermal effect using shell elements. In addition, the thermal effect on the buckling of temperature-dependent nonlinear materials was evaluated. Nonlinear and linear buckling analyses were performed using the arc-length method to investigate the behavioral characteristics of a cylindrical structure. The basic theory of the linear buckling analysis of a cylindrical structure subjected to thermal stress was derived and presented by applying the thermal stress basic theory.

Keywords : Shell Element(쉘요소), Structure Design(구조설계), Finite Element Method(유한요소법), Buckling(좌굴)

1. Introduction

Among the displacement behaviors of structures, buckling is the one that most affects safety and reliability. The buckling point, which is critical for determining the safety and instability of a structure, is used as a reference in designs. Thus, research into it has been conducted over a long period by many researchers[1-5].

Because cylindrical structures are essential elements in designing aircraft and other industrial structures, many analyses have been conducted and articles published on buckling behavior related to these structures. Andre et al.[6] explored post-buckling phenomena, while Shahsiah et al.[7] investigated buckling due to thermal effects and Foroutan et al.[8] conducted a study on dynamic buckling. Buckling analysis is largely divided into nonlinear and linear. Nonlinear buckling analysis typically uses nonlinear analysis methods such as displacement control and arc-length[9] to analyze buckling and post-buckling behavior. On the other

Corresponding Author : hkcho@anu.ac.kr
Tel: +82-54-820-5677, Fax: +82-54-820-6379

hand, linear buckling analysis is used to calculate the unstable buckling point with an initial stress state that is defined based on the vibration mode of the structure. The theoretical background and analysis results of buckling have been clearly formulated, with the latter also being very reliable.

Based on the existing theoretical background, the effect of buckling when a thermal load is applied was investigated in this study. In other words, a theoretical formulation was derived to identify the critical point for buckling of a structure subjected to thermal stress (initial stress) due to temperature rise and its effect evaluated on a cylindrical shell structure. In addition, the post-buckling behavior was calculated by using the arc-length method to clearly identify the nonlinear buckling behavior characteristics of the cylindrical structure, and the results of this analysis were compared with those of the linear buckling analysis with discussion of the differences.

2. Formulation for the Finite Element Analysis (FEA)

2.1 Equilibrium Equation of Degenerated Shell Element

One of the most utilized elements in analyzing 3D structures is the shell element. The shell element can efficiently represent displacements from actions such as bending, shearing, and tension when the number of nodes per element is relatively small. In particular, a shell element having only one node in the thickness direction is called a degenerated shell element. Fig. 1 shows the basic shell elements that are conventionally used.

The formulation of shell elements is clearly defined and has three displacements and three rotational degrees of freedom for each node. This displacement and rotation can be quantitatively represented as

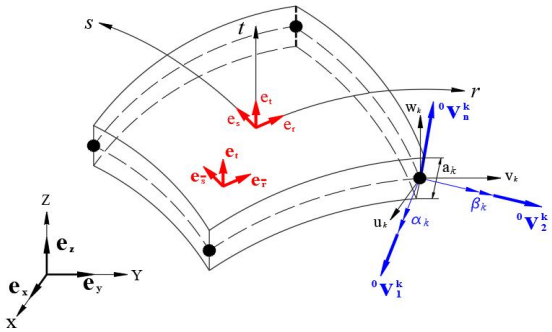

Fig. 1 4-noded shell element configuration

$$ {}^{t}x_i = \sum_{k=1}^{n} h_k \, {}^{t}x_t^k + \frac{t}{2} \sum_{k=1}^{n} a_k h_k \, {}^{t}V_{ni}^k \tag{1} $$

Here, the displacements at time t, 0, and $t+\Delta t$ can be represented as in Equation (2).

$$ {}^{t}u_i = {}^{t}x_i - {}^{0}x_i \tag{2} $$

$$ u_i = {}^{t+\Delta t}x_i - {}^{t}x_i \tag{3} $$

Substituting Equation (1) into Equations (2) and (3) leads to Equation (4) as follows:

$$ {}^{t}u_i = \sum_{k=1}^{N} h_k \, {}^{t}u_i^k + \frac{t}{2} \sum_{k=1}^{N} a_k h_k \left(V_{nt}^k - {}^{0}V_{nt}^k \right) \tag{4} $$

$$ u_i = \sum_{k=1}^{N} h_k u_i^k + \frac{t}{2} \sum_{k=1}^{N} a_k h_k \, V_{ni}^k \tag{5} $$

$$ V_{ni}^k = {}^{t+\Delta t}V_{ni}^k - {}^{t}V_{ni}^k \tag{6} $$

Subsequently, Equation (4) is used to calculate the total displacement. To perform the calculation using Equation (5), it must first be expressed in the form of a direction cosine with respect to the vertical direction of the shell surface. The vertical vector to the tangent vector of the shell represented by ${}^{t}V_1^k$ and ${}^{t}V_2^k$ is ${}^{t}V_n^k$. The following relationship is established between the tangent vector and the vertical vector of the shell,

$$ {}^{t}V_1^k = \left(e_2 \times {}^{t}V_n^k\right) / \left| e_2 \times {}^{t}V_n^k \right| \tag{7} $$

$$ {}^{t}V_2^k = {}^{t}V_n^k \times {}^{t}V_1^k \tag{8} $$

$$ V_n^k = -{}^{t}V_2^k \alpha_k + {}^{t}V_1^k \beta_k \tag{9} $$

where α_k and β_k represent the angles of rotation around the tangent vectors ${}^{t}V_1^k$ and ${}^{t}V_2^k$, respectively. The displacement at each calculation step represented as an incremental formula is as shown in Equation (10). The displacement and rotation angle calculated in the iterative calculation are the data used to calculate the new tangent and vertical vectors in the next step.

$$ u_i = \sum_{k=1}^{N} h_k u_i^k + \frac{t}{2} \sum_{k=1}^{N} a_k h_k \left[-{}^{t}V_{2i}^k \alpha_k + {}^{t}V_{1i}^k \beta_k \right] \tag{10} $$

The vertical vector updated by displacement and rotation is as follows.

$$ {}^{t+\Delta t}V_n^k = {}^{t}V_n^k + \int_{\alpha_k, \beta_k} -{}^{\tau}V_2^k d\alpha_k + {}^{\tau}V_1^k d\beta_k \tag{11} $$

The form of the final equation used for the displacement calculation in the total Lagrangian nonlinear equilibrium equation of shell elements is shown in Equation (12).

$$ \begin{bmatrix} u_{i,r} \\ u_{i,s} \\ u_{i,t} \end{bmatrix} = \sum_{k=1}^{N} = \begin{bmatrix} h_{k,r} \begin{bmatrix} 1 & {}^{t}g_{1i}^k & {}^{t}g_{2i}^k \end{bmatrix} \\ h_{k,s} \begin{bmatrix} 1 & {}^{t}g_{1i}^k & {}^{t}g_{2i}^k \end{bmatrix} \\ h_{k,t} \begin{bmatrix} 1 & {}^{t}g_{1i}^k & {}^{t}g_{2i}^k \end{bmatrix} \end{bmatrix} \begin{bmatrix} u_i^k \\ \alpha_k \\ \beta_k \end{bmatrix} \tag{12} $$

Here,

$$ {}^{t}g_{1i}^k = -\frac{1}{2} a_k^t V_{2i}^k \tag{13} $$

$$ {}^{t}g_{2i}^k = \frac{1}{2} a_k^t V_{1i}^k \tag{14} $$

2.2 Nonlinear Analysis by Applying the Arc-Length Method

Buckling is accompanied by snap-through and snap-back phenomena. When these occur, an incremental nonlinear numerical analysis method is required to clearly calculate the force-displacement relationship behavior of the structure. The arc-length method can be effectively applied in buckling analysis when snap-back occurs. The analysis was performed by using both the arc-length method and the displacement control method. In the arc-length method, the load factor λ for the incremental calculation is used to find a solution through a numerical analysis method, as shown in Fig. 2.

If the number of iterations is i, the step is n and the load factor is λ, which can be expressed as the following nonlinear equilibrium equation.

$$ [K_n^{(i)}]\{\Delta u^{(i)}\} = \lambda\{R_n\} - \{F_n^{(i-1)}\} \tag{15} $$

Representing Equation (15) as an incremental equation becomes Equation (16).

$$ \begin{aligned} [K_i]\{\Delta u^{(i)}\} - \Delta\lambda\{R\} &= \left(\lambda_n + \lambda^{(i)}\right)\{R\} - \{F_n^{(i-1)}\} \\ &= -\{P^{(i)}\} \end{aligned} \tag{16} $$

Displacement for each iteration can be obtained by combining the displacement of parts *I* and *II*.

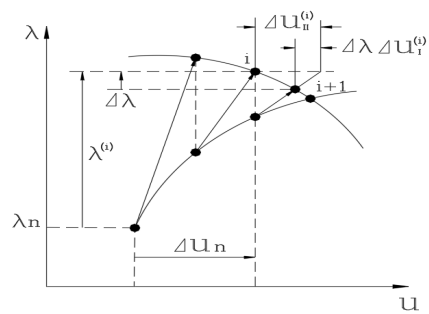

Fig. 2 Arc-length procedure[10]

$$\{\Delta u^{(i)}\}=\Delta\lambda\{\Delta u_I^{(i)}\}+\{\Delta u_{II}^{(i)}\} \tag{17}$$

$$\{\Delta u_{II}^{(i)}\}=-[K^{(i)}]^{-1}\{P^{(i)}\} \tag{18}$$

The vector for the ith iterative calculation connecting the previous and current steps at an arbitrary point is defined as follows.

$$t^{(i)}=\{\Delta u_n\}+\beta\lambda^{(i)} \tag{19}$$

2.3 The Buckling Equation

Linear buckling analysis of a structure is often referred to as eigenvalue buckling analysis because the buckling load is calculated via numerical analysis. The stiffness matrix constructed in the geometrically nonlinear analysis of a structure is divided into a part for elastic energy and a stiffness matrix by geometric nonlinearity. The geometrically nonlinear stiffness matrix is proportional to the load that the structure can support[10].

$$({}_0^tK_L+\phi\,{}_0^tK_{NL})\{u\}=\{{}^{\Delta t}R\} \tag{20}$$

This equation can summarize displacement u as follows.

$$\{u\}=({}_0^tK_L+\phi\,{}_0^tK_{NL})^{-1}\{{}^{\Delta t}R\} \tag{21}$$

Because the displacement is not zero in Equation (21), there is no inverse of the stiffness matrix when assuming an unstable state when buckling occurs, i.e. the critical point at which the displacement becomes infinite and divergent. The relational expression that satisfies this is Equation (22).

$$\det({}_0^tK_L+\phi\,{}_0^tK_{NL})=0 \tag{22}$$

In this case, ϕ refers to the buckling load factor (BLF) obtained through the eigenvalue analysis.

2.4 Thermal Stress FEA

A material that alternately expands and contracts due to heat generates thermal stress according to temperature change. Thermal strain, ϵ^{th}, induces by thermal stress, as represented in the following equation.

$$\epsilon_{xx}^{th}=\alpha(\theta-\theta_0) \tag{23}$$

$$\epsilon_{yy}^{th}=\alpha(\theta-\theta_0)$$

$$\epsilon_{zz}^{th}=\alpha(\theta-\theta_0)$$

$$\gamma_{xy}^{th}=\gamma_{yz}^{th}=\gamma_{zx}^{th}=0$$

The thermal stress resulting from ϵ^{th} is shown as in Equation (24).

$$\tau=C(\epsilon-\epsilon^{th}) \tag{24}$$

Thermal stress is applied after conversion into a load in the nonlinear equilibrium equation. The load equation due to this thermal stress is Equation (25).

$$R_I=\int_V B^T\tau^I dV$$

$$\tau^I=-\frac{E(1-\nu)\alpha}{(1+\nu)(1-2\nu)}$$

$$\begin{bmatrix} 1 & \frac{\nu}{1-\nu} & \frac{\nu}{1-\nu} & 0 & 0 & 0 \\ \frac{\nu}{1-\nu} & 1 & \frac{\nu}{1-\nu} & 0 & 0 & 0 \\ \frac{\nu}{1-\nu} & \frac{\nu}{1-\nu} & 1 & 0 & 0 & 0 \\ 0 & 0 & 0 & \frac{1-2\nu}{2(1-\nu)} & 0 & 0 \\ 0 & 0 & 0 & 0 & \frac{1-2\nu}{2(1-\nu)} & 0 \\ 0 & 0 & 0 & 0 & 0 & \frac{1-2\nu}{2(1-\nu)} \end{bmatrix}$$

$$\times\begin{bmatrix}1\\1\\1\\0\\0\\0\end{bmatrix}\left\{\left(\sum_{i=1}^{8}h_i\theta_i\right)-\theta_0\right\} \tag{25}$$

The total Lagrangian large displacement nonlinear equilibrium equation when considering thermal stress is as follows:

$$\left({}_0^tK_L + {}_0^tK_{NL}\right)\Delta U^{(i)} = {}^{t+\Delta t}R - {}_0^{t+\Delta t}F^{(i-1)} - {}^{t+\Delta t}R_I \quad (26)$$

3. Buckling of the Cylindrical Shell

3.1 Geometry and FEA Modeling

Fig. 3 shows the basic model concept of the cylindrical shell structure. Various boundary conditions are applied to part of the cylindrical structure through a geometric model, and the analysis was performed. In this analysis, the temperature boundary condition was set so that the same temperature acts on the entire structure. For the buckling analysis of the cylindrical shell, the model shown in Fig. 4 was explored. A simply supported boundary condition was given at the edge of the cylindrical shell having a radius of $r = 450mm$, a length of $l = 60mm$, and thickness of $t = 6.35mm$. The Young's modulus (E), Poisson ratio (ν), and thermal expansion coefficient (α) values of a material change linearly with temperature, as reported in Table 1. The FEA model for the cylindrical shell was prepared by using the four-node shell elements described in Section 2.1. The number of elements used was 1,152 and the number of nodes was 1,225.

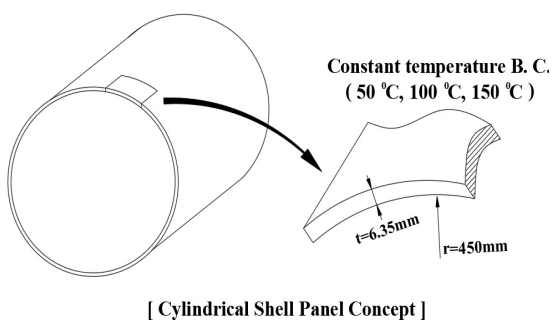

Fig. 3 Cylindrical shell concept and temperature B.C.

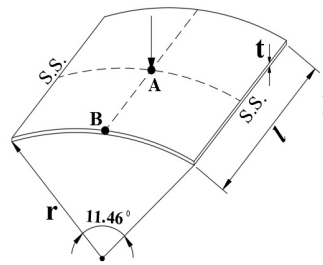

Fig. 4 Cylindrical shell model for buckling analysis

Table 1 Material properties

	Temperature(℃)	
Properties	22	150
E(MPa)	210,000	170,000
ν	0.3	0.26
$\alpha(\mu m/m)$	22.0	17.0

The effect of temperature (thermal stress) on the buckling phenomenon of a cylindrical shell was evaluated in this study. The reference temperature at which the thermal stress becomes zero was 22 ℃. The change in behavior of thermal stress on buckling was calculated at three temperatures: 50, 100, and 150 °C. In this case, the temperature boundary condition was that the same temperature acts on the entire structure. In the case of the cylindrical shell shown in Fig. 4, even when the same temperature condition was applied to the entire structure, the distribution of the stress varies depending on the location because the geometry is curve-shaped. In other words, the maximum thermal stress occurred at the central part of the panel because thermal stress is induced by thermal expansion.

3.2 Thermal Stress and Nonlinear Buckling Analysis

The temperature at which the thermal stress was zero is 22 °C, as reported in the previous section. Prior to the buckling analysis, the respective thermal stresses at 50, 100, and 150 ℃ were as shown in

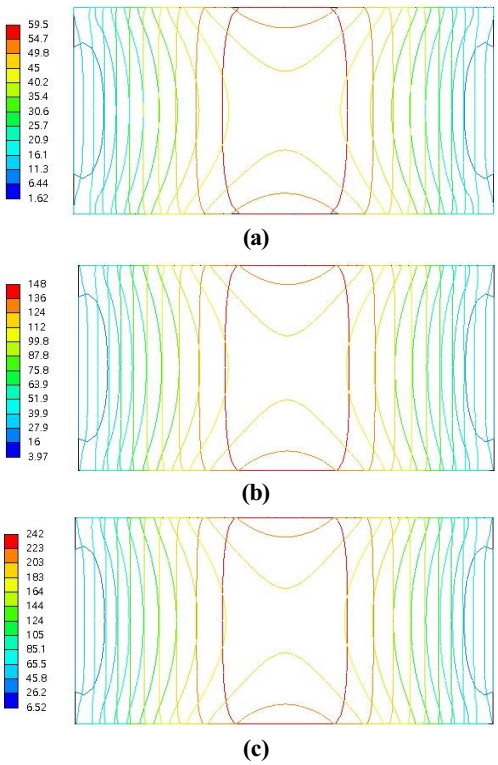

Fig. 5 Thermal stress distribution: (a) 50℃, (b) 100℃, (c) 150℃

Fig. 5. Thermal stress is generated by thermal expansion, and thermal expansion is internally converted into thermal load before the final calculation. At the center, the maximum thermal stress was 59.5 Mpa at 50°C, 148 MPa at 100°C, and 242 MPa at 150°C. Due to the nature of the boundary conditions constrained by a simple support, the displacement due to thermal expansion directly increased the thermal stress, resulting in a considerably high level of stress distribution.

Nonlinear buckling analysis was performed to evaluate the effect of thermal stress on cylindrical shell buckling. Based on the load-displacement relationship at 22 ℃, which is the temperature at which thermal stress does not act, the load-displacement relationships at 50, 100, and 150 ℃ are shown in Fig. 6. As the temperature increased,

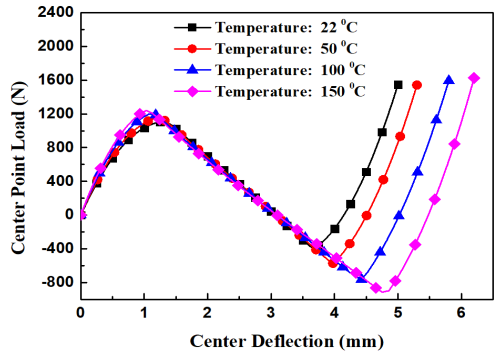

Fig. 6 Displacement vs. load curves for individual temperature conditions

Table 2 Nonlinear buckling load analysis results according to temperature

Temperature (℃)	Displacement (mm)	Buckling load (N)
22	1.33	1,106.3
50	1.24	1,154.7
100	1.08	1,199.5
150	1.03	1,241.6

the magnitude of the thermal stress became higher and the buckling load rose. Table 2 reports the specific temperature, vertical displacement, and buckling load when buckling occurred. At room temperature (22 ℃), buckling occurred when the vertical displacement was 1.33 mm, with a buckling load of 1,106 N. On the other hand, the displacement was 1.03 mm at 150 ℃, with a buckling load of 1,241N, which was around 12.2% higher than the load at room temperature. As shown in Fig. 6, the force was applied in the reverse direction after the critical point of the first buckling had passed. When the force in the reverse direction passed through the second critical point again, the direction of the force was reversed. The displacement and reaction load of the second critical point compared to the first critical point showed significant changes according to temperature. This is a geometrical nonlinear behavioral characteristic that should be particularly noted when designing a

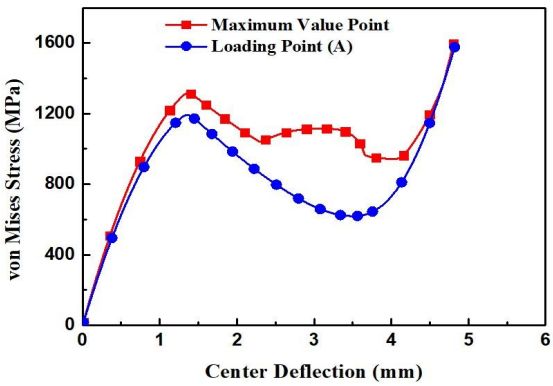

Fig. 7 Stress variation during buckling progress

structure. In other words, because the change in stress at the second critical point is large, it is highly likely to exceed the yield strength of the material. When buckling occurs in geometric nonlinear analysis, it becomes considerably difficult to evaluate the safety of the material. For this reason, it is essential to accurately calculate the maximum stress at the time when buckling occurs. In the case of the cylindrical shell, the stress change during the buckling behavior at room temperature at the point where the buckling load acts is shown in Fig. 7, which indicates that the maximum stress did not occur at the load point during the buckling but instead occurred in the vicinity of the load application point. Snap-through or snap-back are typical buckling phenomena for a curved panel, and irregular or discontinuous stress and displacement can occur during this period. Because the yield strength or fracture strength is instantaneously passed through in nonlinear analysis, a careful review is required when evaluating and diagnosing the safety of a structure.

3.3 Thermal Stress and Linear Buckling Analysis

Linear buckling analysis is used to evaluate the buckling load based on the modal solution of the stiffness matrix, as described in Section 2.3. Modal analysis was performed on the cylindrical shell to determine the solution for the linear buckling load. Table 3 reports the modal frequencies according to each temperature condition.

Table 3 Modal analysis results according to temperature

Mode	Temperature(℃)			
	22	50	100	150
	Frequency (Hz)			
1	1,690.8	1,637.0	1,536.3	1,428.5
2	1,778.5	1,719.9	1,610.8	1,495.0
3	2,065.8	2,002.1	1,882.5	1,753.8
4	3,099.4	3,004.7	2,826.7	2,635.0
5	4,079.7	3,944.0	3,691.9	3,424.7

In the case of no thermal stress, the frequency of the basic primary mode was around 1,690.8 Hz, which varied to 1,637.0, 1,536.3, and 1,428.5 Hz at 50, 100, and 150°C, respectively. As the temperature increased, Young's modulus of the material became lower and the thermal stress rose. Considering the thermal stress and changes in the nonlinear properties of the material, the modal frequency gradually decreased as the temperature increased.

The change of modal frequency with respect to temperature was not relatively large. Table 4 summarizes the linear buckling mode according to each temperature. The results reveal a change in the buckling mode due to the additionally applied heat effect. The comparison between temperatures in the third buckling mode shows the same tendency at 22 and 150 ℃, as well as 50 and 100 ℃.

Because the effect of the buckling mode is exerted as a combination of material property changes, thermal stress, geometry, and boundary conditions, additional research is necessary to independently identify the influence of each variable. However, under the assumption of the same geometry and boundary conditions, the results of this study confirm that thermal stress has a relatively large influence on buckling; linear and nonlinear buckling analysis methods were used to

Table 4 Eigen buckling mode according to temperature

Buckling mode	Temperature 22℃	50℃
1	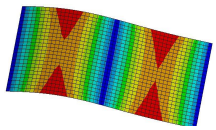	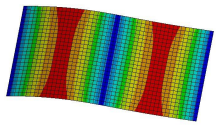
2	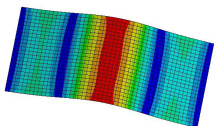	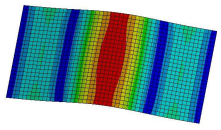
3	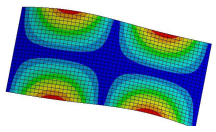	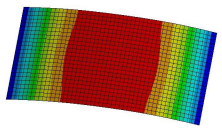

Buckling mode	100℃	150℃
1	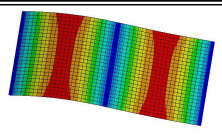	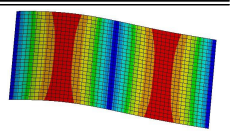
2	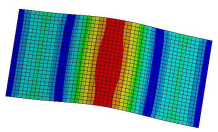	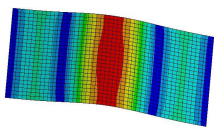
3	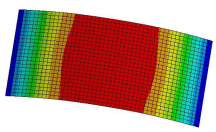	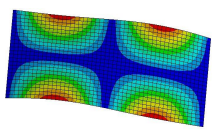

evaluate the influence. Table 5 summarizes changes in the buckling load due to the thermal effect in the linear buckling analysis. These provided the results of calculating BLF ϕ mentioned in Section 2.3 for each variable. The linear buckling load is a value calculated based on the mode and frequency solution from the modal analysis.

Calculating the buckling load was achieved by analyzing it after applying a one-unit load to point A in the shape presented in Fig. 3. Thus, for no thermal stress, the value of buckling load becomes equivalent to BLF ϕ. Under thermal stress, the effect of thermal stress increases by a multiple of

Table 5 Eigen buckling load analysis results according to temperature

	Temperature(℃)			
	22	50	100	150
Mode	Buckling Load Multiplier (ϕ)			
1	1,918.2	24.6	9.7	6.6
2	4,267.5	54.3	21.5	14.6
3	6,389.0	91.1	36.4	24.6
4	7,221.3	92.1	36.5	24.8
5	7,802.5	98.7	39.2	26.5

BLF because the buckling load value is obtained by multiplying the thermal stress and the stress value of the unit load. This can be verified by the fact that the BLF at 50 ℃ was 24.6, which is significantly lower than 1,928.2 with no thermal effect. Due to the cylindrical shell`s geometry, the higher the temperature, the lower the BLF. What is important here is that a lower BLF does not necessarily result in a lower overall buckling load because the value given at prestress is a combination of thermal stress and concentrated load rather than a single concentrated load.

The calculations of buckling load without thermal stress are 1,106.3 N from the nonlinear static numerical analysis (Table 2) and 1,918.2 N from the linear buckling analysis (Table 5); this difference can be attributed to the theoretical background of the numerical analysis. The actual behavior was in good agreement with the nonlinear static numerical analysis. In particular, as the geometrical nonlinearity became stronger in structures such as cylindrical shells, the difference between the results of the two analyses became higher. Because the stiffness matrix of the material changed rapidly as the structure deformed, the nonlinear static numerical analysis, which involves calculations while continuously updating the stiffness matrix, more accurately represents the actual phenomenon. On the other hand, because the buckling load is calculated using the initial stiffness matrix in the case of linear buckling analysis, the calculated and actual

buckling load values were significantly different. However, linear buckling analysis is highly accurate for geometrical structures that are essentially linear.

4. Conclusions

In this study, the buckling phenomenon of a cylindrical structure was analyzed by using four-node shell elements. The results of a numerical analysis regarding the effect of the change in thermal stress on the buckling load due to increasing temperature were presented. Furthermore, it was confirmed that the thermal stress sensitively affects the buckling behavior of the analyzed cylindrical shell. In addition, through the analysis of buckling and post-buckling phenomena by applying the arc-length method and displacement control, the exact displacement under buckling and the load in each case were explicitly calculated according to the change in thermal stress.

By clearly identifying the relationship between thermal stress and buckling when designing a structure where actual buckling occurs, the results of this study can be used as key basic data for reliable structural designs.

Acknowledgments

This work was supported by a Research Grant of Andong National University.

References

1. Cho, H. K., “The Effects of Composite Laminate Layups on Nonlinear Buckling Behavior Using a Degenerated Shell Element,” Journal of the Korean Society of Manufacturing Process Engineers, Vol. 15, No. 1, pp. 50-60, 2016.
2. Thornton, E. A., “Thermal Buckling of Plates and Shells,” Applied Mechanics Review, Vol. 46, No. 10, pp 485-506, 1993.
3. Izhak, S., “Cylindrical Buckling Load of Laminated Columns,” Journal of Engineering Mechanics, Vol. 115, No. 3, pp. 659-661, 1989.
4. Batterman, S. C., “Tangent Modulus Theory for Cylindrical Shells: Buckling Under Increasing Load,” International Journal of Solids and Structures, Vol. 3, No. 4, pp. 501-512, 1967.
5. Hieu, P. T. and Hoang, V. T., “Thermomechanical Postbuckling of Pressure-loaded CNT-Reinforced Composite Cylindrical Shells under Tangential Edge Constraints and Various Temperature Conditions,” Polymer Composites, Vol. 41, No. 1, pp. 244-257, 2020.
6. Andre, M. and Nuno, D. S., “Modal analysis and Imperfection Sensitivity of the Post-buckling Behaviour of Cylindrical Steel Panels under In-plane Bending,” Engineering Structures, Vol. 207, No. 15, 2020.
7. Shahsiah, R. and Esiami, M. R., “Thermal Buckling of Functionally Graded Cylindrical Shell,” Journal of Thermal Stress, Vol. 26, No. 3, pp. 277-294, 2011.
8. Foroutan, K., Shaterzadeh, A. and Ahmadi, H., “Nonlinear Static and Dynamic Hygrothermal Buckling Analysis of Imperfect Functionally Graded Porous Cylindrical Shells,” Applied Mathematical Modeling, Vol. 77, pp. 539-553, 2020.
9. Zhu, J. F. and Chu, X. T., “An Improved Arc-length Method and Application in the Post-buckling Analysis for Composite Structures,” Applied Mathematics and Mechanics, Vol. 23, pp. 1081-1088, 2002.
10. Hughes, T. J. R. and Liu, W. K., “Nonlinear Finite Element Analysis of Shells: Part I. Three-Dimensional Shells,” Computer Methods in Applied Mechanics and Engineering, Vol. 26, No. 3, pp. 331-362, 1981.